OPEN ACCESS
IOP Publishing
Plasma Sources Science and Technology
Plasma Sources Sci. Technol. **31** (2022) 105005 (13pp)
https://doi.org/10.1088/1361-6595/ac942a

Hydrogen peroxide production of underwater nanosecond-pulsed streamer discharges with respect to pulse parameters and associated discharge characteristics

Raphael Rataj[1,2], Matthias Werneburg[1,3], Harald Below[4] and Juergen F Kolb[1,2,*]

[1] Leibniz Institute for Plasma Science and Technology (INP), Felix-Hausdorff-Str. 2, 17489 Greifswald, Germany
[2] University of Rostock, Institute of Physics, Albert-Einstein-Str. 23-24, 18059 Rostock, Germany
[3] University of Greifswald, Institute of Physics, Felix-Hausdorff-Str. 6, 17489 Greifswald, Germany
[4] Department of Restorative Dentistry, Periodontology, Endodontology, Preventive and Pediatric Dentistry, Dental School of University Medicine Greifswald, Walter-Rathenau-Straße 42, 17489, Greifswald, Germany

E-mail: raphael.rataj@inp-greifswald.de and juergen.kolb@inp-greifswald.de

Received 1 June 2022, revised 15 August 2022
Accepted for publication 22 September 2022
Published 14 October 2022

Abstract

Pulsed streamer discharges submerged in water have demonstrated potential in a number of applications. Especially the generation of discharges by short high-voltage pulses in the nanosecond range has been found to offer advantages with respect to efficacies and efficiencies. The exploited plasma chemistry generally relies on the initial production of short-lived species, e.g. hydroxyl radicals. Since the diagnostic of these transient species is not readily possible, a quantification of hydrogen peroxide provides an adequate assessment of underlying reactions. These conceivably depend on the characteristics of the high-voltage pulses, such as pulse duration, pulse amplitude, as well as pulse steepness.

A novel electrochemical flow-injection system was used to relate these parameters to hydrogen peroxide concentrations. Accordingly, the accumulated hydrogen peroxide production for streamer discharges ignited in deionized water was investigated for pulse durations of 100 ns and 300 ns, pulse amplitudes between 54 kV and 64 kV, and pulse rise times from 16 ns to 31 ns. An independent control of the individual pulse parameters was enabled by providing the high-voltage pulses with a Blumlein line. Applied voltage, discharge current, optical light emission and time-integrated images were recorded for each individual discharge to determine dissipated energy, inception statistic, discharge expansion and the lifetime of a discharge.

Pulse steepness did not affect the hydrogen peroxide production rate, but an increase in amplitude of 10 kV for 100 ns pulses nearly doubled the rate to (0.19 ± 0.01) mol l^{-1} s^{-1}, which was overall the highest determined rate. The energy efficiency did not change with pulse

* Author to whom any correspondence should be addressed.

amplitude, but was sensitive to pulse duration. Notably, production rate and efficiency doubled when the pulse duration decreased from 300 ns to 100 ns, resulting in the best peroxide production efficiency of (9.2 ± 0.9) g kWh^{-1}. The detailed analysis revealed that the hydrogen peroxide production rate could be described by the energy dissipation in a representative single streamer. The production efficiency was affected by the corresponding discharge volume, which was comprised by the collective volume of all filaments. Hence, dissipating more energy in a filament resulted in an increased production rate, while increasing the relative volume of the discharge compared to its propagation time increased the energy efficiency.

Keywords: hydrogen peroxide, nanosecond-pulsed streamer, pulsed power, plasma in liquids, plasma chemistry

S Supplementary material for this article is available online

(Some figures may appear in colour only in the online journal)

1. Introduction

Sub-microsecond pulsed streamer discharges in liquid water, which are generated from the application of high-voltage pulses, have been found an environmentally friendly technology to degrade hazardous pollutants [1–4]. In general, this water purification method exploits the generation of UV-radiation and oxidative chemical species, e.g. ·O, ·OH or ·OOH. Especially, hydroxyl radicals are known for their high reactivity and, hence, their essential role in the plasma-assisted degradation of recalcitrant organic compounds. However, hydroxyl radicals are short-lived with a lifetime in the order of milliseconds at most [5]. Unless they react with other compounds, i.e. pollutants, the radicals eventually recombine to hydrogen peroxide. Therefore, in particular in pure water, the more stable hydrogen peroxide concentration is an appropriate measure for initially created hydroxyl radicals [6, 7].

Recent publications reported hydrogen peroxide production efficiencies for sub-microsecond pulsed streamer discharges in liquid water of (1–2) g kWh^{-1}, which is low when accounting for the limitations on treatment costs in common sewage water treatment plants [6–9]. An optimization of electrical operating parameters is an obvious way to improve the efficiency of pulsed power systems. However, this requires a detailed understanding of the influence of pertinent electrical characteristics [8, 10].

Sub-microsecond pulsed streamer discharges in liquid water are typically instigated by rectangular high-voltage pulses, which can be described by direct and derived parameters. Direct parameters, such as amplitude, pulse steepness and pulse duration, define the shape of an individual pulse, while derived parameters, like energy and repetition rate, characterize the pulses in relation to the specific experimental conditions, e.g. implicitly consider pulse reflections due to impedance mismatching or inherently include discharge or residual post-discharge characteristics. Derived parameters, especially energy, have generally been investigated with respect to specifically pursued applications [6–9, 11]. Only few fundamental studies have considered the effect of selected direct parameters on hydrogen peroxide production [9–23].

For example, increasing pulse amplitudes have been observed to accelerate the production. The finding is commonly explained with an increased power density in a streamer, resulting in higher channel temperatures [9, 11–16]. Concurrent simulations showed that the thermal dissociation of H_2O in the discharge filaments was the dominant pathway for creating hydroxyl radicals [9, 17]. Accordingly, higher temperatures should correspond to higher amounts of hydrogen peroxide. However, a higher pulse amplitude also resulted in an earlier discharge-onset [18–21]. Accordingly, streamer lengths were increasing with an earlier ignition, yielding higher amounts of chemical species even if the channel temperature was not rising [10, 22]. Therefore, species concentrations cannot be understood solely from the direct parameters. In addition, the discharge characteristics (with respect to the properties of the propagation medium, like conductivity), e.g. streamer length, morphology, temperature, time lags, etc, have to be taken into account.

A pertinent example is the effect of pulse duration, which dominantly affects the streamer length and statistical time lag for a given electrode configuration [10, 22]. Associated is an enlarged active discharge volume, which encouraged the production of higher amounts of hydrogen peroxide [10, 11, 16].

Pulse rise times have also been reported crucial for the discharge initiation [23], while fall times have been found to affect post-discharge behavior, i.e. the reillumination of discharge channels [20, 24]. Related effects can consequently be expected on radical reaction chemistry and hydrogen peroxide production.

Although the impact of direct pulse parameters cannot be doubted, comprehensive studies on their individual contribution to the promoted plasma chemistry are so far insufficient. Previous reports have either focused on a specific characteristic, mostly neglecting the relation to other aspects, in particular

of the treated medium, e.g. conductivity, or have fallen short to consider the impact of a specific parameter also on other possibly affected discharge characteristics, e.g. time lags, or lacked the necessary single discharge diagnostic, i.e. electrical and optical methods, to resolve individual effects [9–21].

Necessary experiments are admittedly challenging and often not possible with the pulsed power systems that were utilized. Exemplary, an increase in amplitude is also associated with longer pulse durations and fall times for high-voltage pulses that are obtained from the discharge of a bulk capacitor [25]. Another example is a mismatch of the load, which results in pulse reflections especially for the application of rectangular high-voltage pulses, which can considerably affect radical chemistry [9].

These challenges were resolved for the presented study by a Blumlein line pulse generator. If correctly matched to the load, the system can provide single, rectangular high-voltage pulses, i.e. without reflections (within limits). A careful consideration of the entire electrical circuit further provided the possibility to include elements, e.g. impedance elements, which allowed for an independent adjustment of pulse duration, pulse amplitudes as well as rise and fall times [24]. The applied and investigated high-voltage pulses were characterized by rise and fall times in a range from (16–31) ns and (21–37) ns, respectively. Pulse amplitudes were adjusted from (54–64) kV and pulse durations set to 100 ns or 300 ns.

Accordingly, individual effects of each direct pulse parameter on the hydrogen peroxide production could be disentangled and related to the underlying development of discharges. Individual discharge events were electrically and optically analyzed to determine dissipated energy, propagation time and streamer length. Hydrogen peroxide concentrations were measured with an electrochemical flow injection analysis (FIA), from which the production efficiencies were summarily calculated.

2. Experimental setup

A schematic of the experimental setup is shown in figure 1, indicating discharge chamber, pulse generator, electrical and optical diagnostics, and typical signals for voltage figure 1(A), current figure 1(B), and light intensity figure 1(C).

2.1. Discharge generation

As previously reported in detail [24], discharges were ignited at a tip with a curvature radius of 35 µm of an otherwise insulated tungsten needle electrode (*Metall Maier*, 99.95% purity) of 2 mm in diameter. The counter electrode was a titanium plate (*Selfan Fine + Metal GmbH*, 99.5%) with a diameter of 46 mm, which was set at a distance, d, of either 8 mm or 14 mm beneath the needle tip. Both electrodes were placed in the middle of a cylindrical chamber with a diameter of 20 mm made from polymethylmethacrylat. The volume was filled with deionized water, which was moved at a flow rate of 120 ml min^{-1} from bottom to top. A total volume of 75 ml of water was circulated.

Rectangular high-voltage pulses were applied with pulse durations, t_{pulse}, of 100 ns and 300 ns by two different, custom-built Blumlein line generators with pressurized spark gaps as closing switches. For the application of 100 ns pulses, pulse amplitudes, U_{mean}, could be adjusted between 54 kV and 64 kV (calculated as the average of voltages, which exceeded 90% of the highest applied voltage during a pulse). The edge steepness of the applied pulse could be modified by means of an adjustable inductance in parallel to the spark gap switch yielding rise times, t_{rise}, of 16 ns, 22 ns and 31 ns and concurrent fall times, t_{fall}, of 21 ns, 29 ns and 37 ns (both defined as the time that amplitudes changed from 10% to 90% of the highest applied voltage). For the application of 300 ns pulses, the amplitude was set at 61 kV and rise time and fall time to 10 ns and 23 ns, respectively. The voltage that was provided by both pulse generators was applied so that the needle was on a positive and the plate electrode on a negative potential with respect to the ground reference. A matching resistor of 250 Ω, connected in parallel to the electrodes, was chosen to prevent pulse reflections and deliver only single, well-defined pulses with a repetition rate of 1 Hz.

2.2. Electrical and optical diagnostics

The electrical and most of the optical diagnostics were similar to the setup described before [24]. High-voltage pulses were recorded according to the potential difference that was derived from the measurements of two passive high-voltage probes (*Tektronix*, P6015A) at either electrode. Typical recorded voltage signals for single pulses with a pulse duration of 100 ns and fall times of 21 ns, 29 ns or 37 ns are presented in figure 1(A) where also definitions for pulse amplitude, rise time, fall time and duration are indicated.

Corresponding current signals are shown in figure 1(B), which were measured with a Rogowski coil (*Magnelab*, CT-E2.5). The currents were corrected for displacement currents and Ohmic losses, which were derived from applied pulses that did not result in a visible discharge, as confirmed by the simultaneously recorded light emission. Accordingly, signals presented in figure 1(B) only show values for the actual discharge currents. Discharge current and corresponding voltage signal were multiplied and time-integrated to calculate the momentary electrical power and dissipated energy, respectively.

Emitted visual light intensity, I_L, was observed with a photodetector (*ThorLabs*, DET 10A). Typical results are shown in figure 1(C) for different fall times. In addition, characteristic times for discharge ignition, t_{start}, for discharge propagation, Δt, and the onset of discharge channel reillumination, t_{min}, are indicated. The reillumination is a typical observed phenomenon, which marked the end of the propagation of discharge filaments and corresponded to a change in polarity of the discharge current. A more detailed discussion of the electrical and optical signals was provided previously [24].

Together with the photodetector signals, temporal integrated images of the discharge development and especially the expansion were recorded with an ICCD camera (*Stanford Computer Optics*, 4Picos). Gate times of 200 ns and

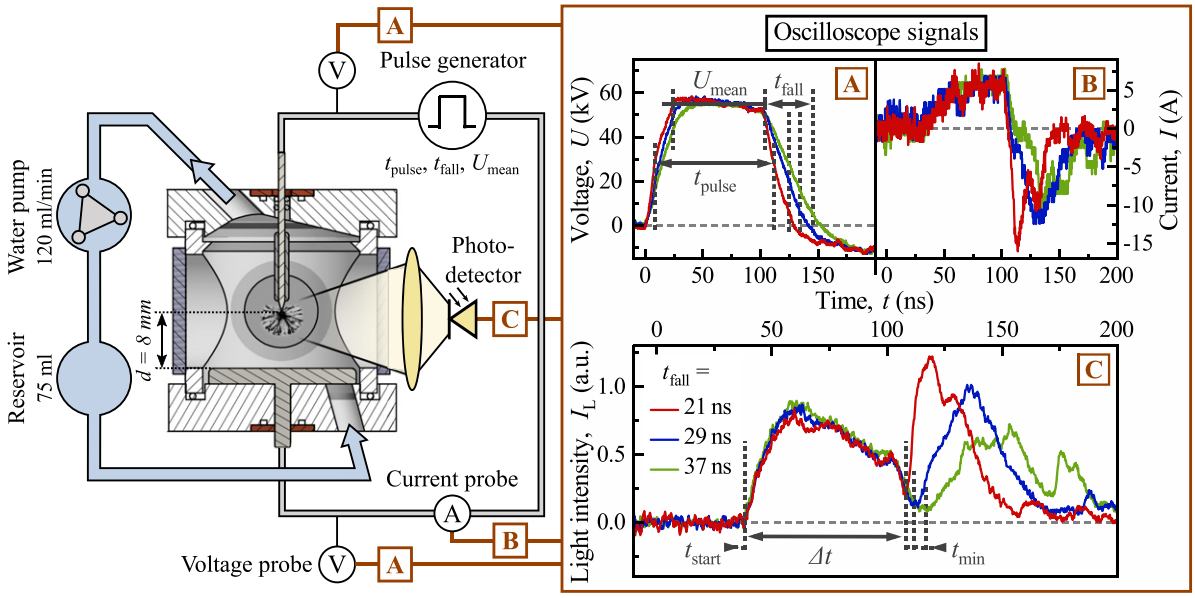

Figure 1. Schematic of the experimental setup, consisting of discharge chamber, pulse generator and diagnostics. Discharges were ignited in a needle-to-plate electrode configuration (submerged in water) with an interelectrode distance, d, and instigated by high-voltage pulses provided by a Blumlein line generator. Deionized water was circulated through the system by a peristaltic pump. Pulse amplitude, U_{mean}, pulse duration, t_{pulse}, pulse rise time, t_{rise}, and fall time, t_{fall}, were recorded in a differential measurement with two high-voltage probes (A), a Rogowski coil (B), and a photodetector (C). Typical signals for voltage (panel (A)), discharge current (panel (B)) and emitted light intensity (panel (C)) are shown for pulse steepnesses characterized by fall times of 21 ns, 29 ns and 37 ns. Images of every discharge event were recorded with an ICCD camera.

600 ns were chosen for pulses of 100 ns and 300 ns duration, respectively. Consequently, image acquisition times covered the entire propagation and reillumination phase for a discharge. Because discharges had stopped expanding when the reillumination began, the images show in particular the largest extend of the discharge. The previously used image analysis algorithm was improved and now detected end points and the length, $L_{s,i}$, of each discharge filament by tracing the brightest path connecting the needle electrode with individual end points (cf figure S1) [24].

2.3. Electrochemical determination of hydrogen peroxide

Concentrations of hydrogen peroxide that were generated by the discharges were quantified electrochemically with a FIA method, which was combined with a chronoamperometric detection [26, 27]. Experiments were performed with screen-printed three-electrode-systems (*Metrohm*, DRP-710) consisting of a working electrode functionalized with Prussian blue, a carbon counter electrode, and a silver reference electrode. A working potential of −0.1 V was applied to the system and reaction currents were measured with a sampling rate of 20 s^{-1} by a potentiostat (*Metrohm*, PGSTAT101).

Water was pumped through the discharge chamber for each experiment for 5 min without the instigation of any discharges before a reference sample of 4.5 ml was taken. After the discharges were applied, another sample was collected and both aliquots were separately mixed with 0.5 ml concentrated buffer solution (134.04 g l^{-1} KH_2PO_4 + 2.67 g l^{-1} Na_2HPO_4 + 74.52 g l^{-1} KCl dissolved in deionized water) containing phosphate to stabilize the H_2O_2-concentration. Both samples were then stored in a refrigerator until the electrochemical measurements were conducted at the end of each day for all sample-pairs that were collected for different operating parameters. The earliest obtained samples were stored for 6 h at most. A control experiment showed no effects, i.e. increase or decrease in hydrogen peroxide concentrations, for continuous pumping for 1 h without discharge or storage of the solution for 10 h.

After all samples for an experimental series were gathered, a chip electrode was installed in the FIA-setup, moistened with running buffer and activated with several consecutive cyclic-voltammetric measurements until a stable voltammogram was obtained. A dilution of the concentrated buffer of 10% was used as running buffer. A calibration curve was then obtained by injecting hydrogen peroxide standard solutions of increasing concentration, i.e. (1, 2, 4, 6, 8, 10 and 15) µmol l^{-1} H_2O_2 in running buffer, with three repetitions for each concentration. If a linear fit with a Pearson coefficient, R, of at least 0.999 was achieved, 500 µl of reference and treated samples were injected into the FIA-system with five repetitions for each sample. This was followed by two injections of a higher concentrated standard solution (either (8, 10 or 15) µmol l^{-1}) to perform a single peak calibration after the analysis of each sample to ensure electrode stability.

A detection limit of 0.2 µmol l^{-1} and a recovery rate of 98.4% was achieved for a H_2O_2 concentration of 1 µmol l^{-1}. However, no sample with a concentration of less than 2 µmol l^{-1} was obtained in the experiments.

Hydrogen peroxide production rate and efficiency was derived for each experiment separately using H_2O_2 concentration and electrical as well as optical data. Discharge energy and propagation time of the individual discharge events were accumulated and related to the concentrations.

3. Results

Hydrogen peroxide production rate, k, and production efficiency, G, were characterized with respect to pertinent parameters of the high-voltage pulses that were applied to generate sub-microsecond pulsed streamer discharges in liquid water. An obvious influence was expected especially for pulse duration, t_{pulse}, and pulse amplitude, U_{mean}. Both determine to a large extend the discharge development, i.e. propagation time, Δt, and streamer length, L_{s}. The extend and duration of discharges are assumed to be predominantly responsible for the production of reactive species that are preceding the formation of hydrogen peroxide. However, both direct parameters together also affect time lags before discharge initiation, which is described by the inception time, t_{start}. Resulting characteristics of discharge propagation and associated inception probabilities consequently need to be taken into account for a comprehensive description. Concurrently, pulse steepness, expressed by rise and fall time, t_{rise} and t_{fall}, are parameters, which determine in particular reillumination processes and their contribution to the generation of species. The influence of the different factors on hydrogen peroxide production in relation to the responsible discharge characteristics are described in the subsequent sections.

3.1. Hydrogen peroxide production efficiency increases with shorter pulse duration

Two pulse generators with different pulse durations of 100 ns and 300 ns were utilized to observe differences in discharge inception, discharge propagation, as well as the reillumination of discharge filaments after pulse application. The respective processes were related to the accumulated hydrogen peroxide production.

Due to the extended pulse duration, discharge filaments that were developing for 300 ns pulses were expected to by three times longer than for 100 ns pulses. To prevent arcing, the distance between needle and counter electrode was increased to 14 mm for the experiments with both pulse generators. Accordingly, pulse amplitudes were increased to 61 kV so that the electric field at the tip of the needle, which determines the onset of ionization mechanisms, was for the larger electrode gap the same as for the previously investigated shorter gap [24].

Reillumination is a characteristic phenomenon of submicrosecond pulsed streamer discharges in liquid water, which is predominantly determined by fall times (cf figure 1). However, the reilluminated channels were already established during the application of the high-voltage pulses, depending on their respective parameters, i.e. pulse duration and amplitude. Therefore, the contribution of reillumination to hydrogen peroxide production was, in general, inherently included in the comparison of pulse durations. However, for 100 ns pulses it was further investigated in more detail (and described in subsection 3.3). The results for the comparison of pulse durations are summarized in figure 2.

Typical images of single discharge events are presented in figure 2(A) for the application of pulses of both durations. All discharges showed filamentary structures, regardless of pulse duration, contained several channels and propagated into the medium away from the needle. Filaments ignited during a 300 ns pulse were, as expected, noticeably longer with more pronounced elotrophy toward the counter electrode when compared with the application of 100 ns pulses. Filaments propagating toward the counter electrode appeared more intense and branched more often with increasing distance to the needle electrode.

The individual streamer length, L_{s}, that was derived from the images of single discharge events (altogether 200 images for a duration of 100 ns and 400 images for a duration of 300 ns), depending on individual propagation times, Δt, are presented in figure 2(B). An algorithm analyzed all images and determined the distance, $L_{\mathrm{s,i}}$, between the end of each filament and the needle tip (cf figure S1). For the application of 100 ns high-voltage pulses, streamer lengths fluctuated strongly between different discharge events. This was also a consequence of two-dimensional mapping of the discharge, which resulted in a loss of spatial information. A seemingly short filament could either actually be shorter or have propagated out of the imaging plane. Commonly, streamer lengths were determined as the maximal distance of the needle electrode to the end of a single filament [28, 29] or, on average, to the end of every filament end [24, 30]. Both methods neglect the structure of filaments, e.g. changing propagation directions due to branching. For a more precise measurement, the algorithm traced the luminous filaments from end to needle tip and determined the maximum streamer length, L_{s}, to sufficiently describe the discharge expansion. The streamer length, generally, grew linearly with propagation time for both pulse durations with similar growth rate, which could be described by the fitted averaged, constant propagation velocity, v_{s}, of (31.2 ± 0.6) km s^{-1}.

The probability distribution for the inception of discharges, i.e. start time, t_{start}, during the application of a pulse, is shown in figure 2(C). A representative pulse for each pulse duration is indicated in arbitrary units. Whereas the amplitude stayed close to the same value for a pulse duration of 300 ns (plateau), was the amplitude for the 100 ns pulse gradually decreasing by 9%. More than 30% of the discharges were ignited at the beginning of the 100 ns pulse, i.e. 32 ns into the pulse, where the pulse voltages reached the highest values. The probability for a discharge inception decreased for later times. Notably, the inception of discharges started later into the pulse for a duration of 300 ns with a maximum probability of 11% at 71 ns. This was observed despite the faster rise time of 10 ns in comparison to 16 ns for the 100 ns pulse. The distribution for the longer pulse was also broader and a second, local probability maximum can be observed around 250 ns into the pulse. The observed statistics suggest that, besides rise times,

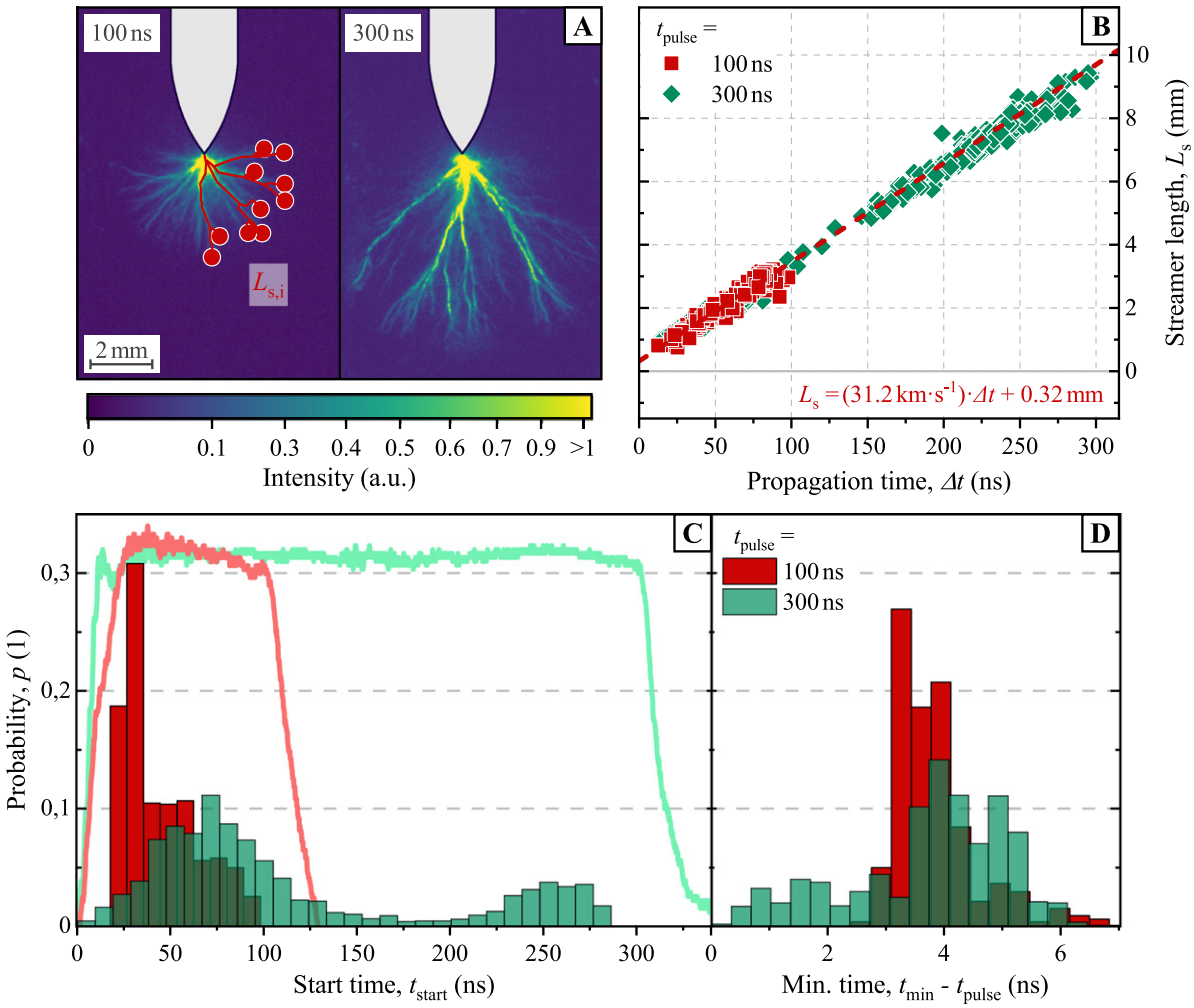

Figure 2. Images of discharge developments (panel (A), for the presentation, only half of the detected streamers are shown), from the images derived maximum streamer length, L_s, depending on propagation time, Δt, (panel (B)), inception time statistic, and reillumination time probability, p, (panel (C) and (D), respectively) for pulse durations of 100 ns (red symbols, lines and bars) and 300 ns (green symbols, lines and bars). The analysis included 200 discharges for the shorter and 400 discharges for the longer pulse duration. Streamer lengths increased linearly with propagation time and a fit yielded a mean propagation velocity, v_s, of (31.2 ± 0.6) km s^{-1}. The probability distribution of inception times corresponded to the pulse shapes, while the distribution for the onset of reillumination was not correlated with the pulse durations.

even small variations of pulse amplitudes could affect inception probability. A longer sustained and invariable amplitude seemed to encourage a broader distribution. With even slightly increasing voltages, there was also an increasing possibility to initiate discharges even late into the pulse.

The pulses had similar fall times of 21 ns and 23 ns for durations of 100 ns and 300 ns, respectively. Since reillumination is primarily determined by fall times, the statistic for the start of the reillumination of discharge filaments after pulse application, as expressed by the difference between t_{min} and t_{pulse} (cf figure 1), was similar for both pulse durations. The probability distribution peaked between 3 ns and 4 ns.

As shown in figure 2(A), filaments were approximately spherically distributed for 100 ns pulses. Spatial distributions were similar for the application of 300 ns pulses for equivalent propagation times. The continuing propagation showed a strong directionality toward the counter electrode for longer propagation times. Only streamers propagating within a ±20°-angle relative to the needle axis reached a length of 7.5 mm (assuming a constant propagation velocity, cf figure 2(B)). For larger angles, especially >|±70|°, streamer lengths of 2.5 mm were on the same order as for the propagation for 100 ns pulses. Accordingly, these streamers stopped their propagation early during the pulse. Details on the directionality and related spatial distributions of filaments are described in the supplemental information (cf figure S2).

The expanse of the discharge and the number of filaments that were generated conceivably determined the possible abundance of chemical reactions and the associated absolute production of reactive species. The parameters for spatial extend and distribution of discharge channels can be summarized by the discharge volume, V_D, which is described in figure 3 with respect to propagation time, Δt, for both pulse durations. For a comparison, the area of light emission in a particular image

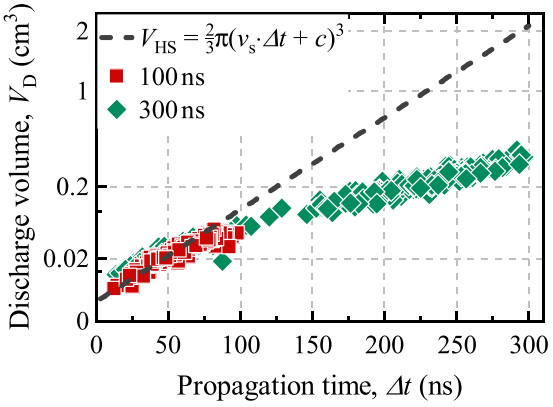

Figure 3. Discharge volume, V_D, associated with propagation time, Δt, for pulse durations of 100 ns and 300 ns. The derivation of the idealized equivalent half-sphere volume, V_{HS}, with radius L_s assumed a continuous expansion with a velocity v_s. The correlation of L_s with Δt was extracted from the measurements summarized in figure 2(B). Accordingly, discharge volumes grew proportional to L_s^3, i.e. cubical, but the growth rate declined after the first 100 ns of propagation.

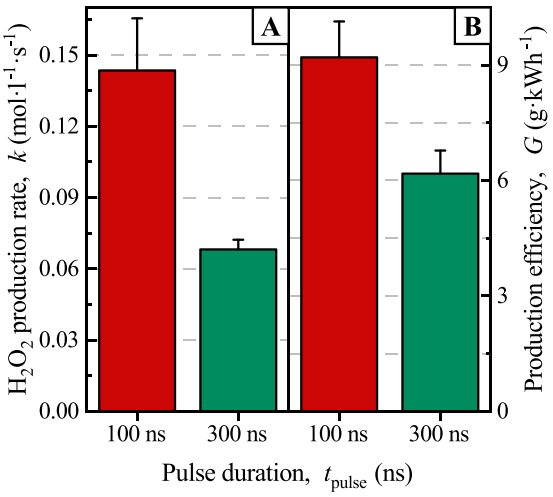

Figure 4. Rate (panel (A)) and efficiency (panel (B)) of hydrogen peroxide production for pulse durations of 100 ns and 300 ns. Both, rate and energy efficiency, increased for a shorter pulse duration.

(cf figure 2(A)) was determined by defining an arbitrary intensity limit (independent of absolute intensity values).

Discharges were generally expanding into a half-sphere away from the needle tip within an ideal volume, V_{HS}. The increasing volume could be calculated from the correlation of streamer lengths, L_s, to the propagation time of discharges, Δt (defined in figure 2(B)). Accordingly, discharge volumes were increasing with distance in a similar cubic fashion for 100 ns and 300 ns pulses for propagation times up to 100 ns. The subsequent later development for the longer pulses approximately retained the spherical propagation but with a slower growth rate (reflecting the described directionality). The resulting discharge volume was, therefore, much smaller than expected from the early propagation. Comparing the discharge volume, V_D with V_{HS}, discharges propagating for 300 ns filled a 80% smaller volume than expected from an expansion of a half sphere with constant velocity.

The rate of energy dissipation into discharge processes differed for both pulse durations regardless of comparable pulse amplitudes. Energy dissipation rates of 0.16 mJ ns^{-1} and 0.12 mJ ns^{-1} were measured for pulses of 100 ns and 300 ns, respectively. Notably, energy dissipation rates were smaller for longer pulses and altogether smaller than those described for an electrode distance of 8 mm.

Discharge volume and energy dissipation affected the observed hydrogen peroxide production and especially explain production rates and efficiencies that are shown in figure 4. Production rates and efficiencies were calculated with respect to the accumulated propagation time and energy dissipation of the discharges that were resulting in the determined hydrogen peroxide concentrations (for the application of either 200 or 400 pulses of the same operating parameters for pulse durations of 100 ns and 300 ns, respectively). The production rate, presented in figure 4(A), was approximately two times higher at (0.14 ± 0.02) mol l^{-1} s^{-1} for the three times shorter pulse. The energy efficiency, shown in figure 4(B), was less affected. The production efficiency of hydrogen peroxide was (9.2 ± 0.9) g kWh^{-1} and (6.2 ± 0.6 g kWh^{-1}) for a duration of 100 ns and 300 ns, respectively. Hence, even the reduced energy dissipation for longer propagation times did not counterbalance the reduced hydrogen peroxide production.

3.2. Hydrogen peroxide production rates increase linearly with pulse amplitude

The energy, provided to a discharge during a pulse is, for a given pulse duration, foremost determined by the pulse amplitude. Corollary, higher amplitudes promote earlier discharge inceptions and a higher probability for the generation of a discharge in general. However, in many respective investigations was the actual applied amplitude of a pulse strongly affected by the load, i.e. in the case of sub-microsecond pulsed streamer discharges in liquid water especially by water conductivity. Accordingly, pulse amplitudes are not necessarily corresponding to the output-settings of many pulse generators, which are usually designed for specific loads. Therefore, instead of a single pulse, reflections often disturb an unambiguous analysis of the influence of pulse amplitudes. A comprehensive understanding on how amplitudes affect hydrogen peroxide production is, hence, difficult. Consequently, a dedicated setup was established, which does not suffer from these limitations by controlling the impedance match between pulse generator and load together with differential measurements of the applied voltage.

Figure 5 shows the dependency of dissipated energy, E, mean start time, t_{start}, and H_2O_2 production rate, k, on pulse amplitude, U_{mean}, in a range from 54 kV to 64 kV for single, well-defined pulses with a duration of 100 ns. Respective results were determined for 500 discharges for each value of the amplitude. For an unambiguous comparison, pulses with the steepest possible rise and fall time of 16 ns and 21 ns, respectively, were applied for an electrode distance of 8 mm. Accordingly, discharge inception was only affected by the variation of pulse amplitudes. Dissipated energies for

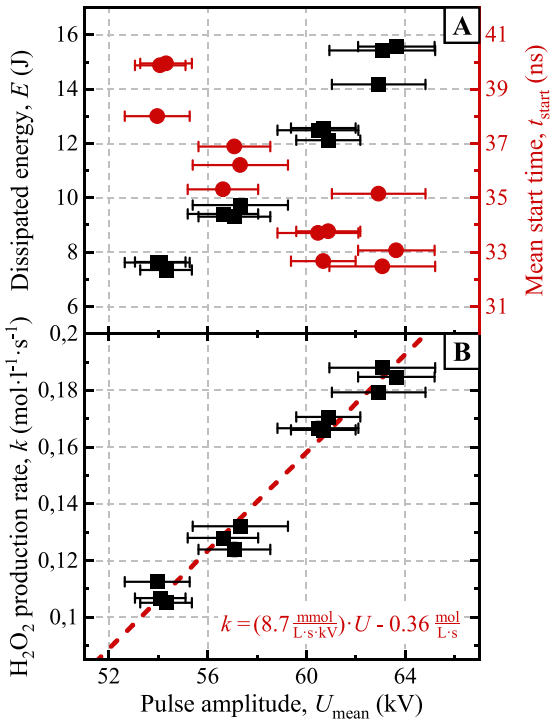

Figure 5. Total energy, E, dissipated for 500 accumulated discharges that were generated with 100 ns high-voltage pulses and their average starting time, t_{start}, (panel (A)) are shown together with hydrogen peroxide production rate, k, (panel (B)) for pulse amplitudes, U_{mean}, between 54 kV and 64 kV. Accumulated discharge energy and production rate increased linearly with pulse amplitude, while the mean starting time decreased.

each individual discharge were accumulated throughout the experiment and correlated with production rates, which were calculated from the sum of discharge propagation times of each set of the 500 investigated discharges and the amounts of H_2O_2 that were formed accordingly.

The accumulated dissipated energy during discharge propagation increased linearly in a range from 8–16 J within the observed range of pulse amplitudes, as displayed in figure 5(A). The rate of energy dissipation, which is also linearly dependent on the pulse propagation time [24], increased by 100% from (0.21 ± 0.04) mJ ns^{-1} to (0.39 ± 0.08) mJ ns^{-1}. Simultaneously, the averaged starting time shortened from 39 ns to 32 ns, which corresponds to an average propagation time extended by 10%.

Hence, the difference in discharge inception could not be exclusively responsible for the observed increase in energy dissipation. Concurrently, the ignition probability of a discharge during a high-voltage pulse also increased with voltage. Starting at 47% for 54 kV, discharges occurred in 87% of all applied pulses with amplitudes of 64 kV. The significance of pulse amplitudes was already implicitly addressed by the statistics that were observed for different pulse durations as presented in figure 2(C). Concurrently, the lowest voltages that were applied with a 100 ns pulse were just sufficient to initiate a discharge. Associated with the low voltages were broadened inception time probability distributions.

As expected, hydrogen production rates were increasing with voltage and the associated higher energy dissipation, as shown in figure 5(B). Notably, the rates nearly doubled from 100 mmol l^{-1} s^{-1} to 190 mmol l^{-1} s^{-1} although the increase in pulse amplitude by about 19% was rather moderate. Applied amplitudes were prone to variations of approximately 4%, but a linear dependency was clearly identified and a fit yielded a growth rate of (8.7 ± 0.4) mmol l^{-1} s^{-1} kV^{-1}. The dependency of voltage with energy dissipation explains a stable, i.e. constant, production efficiency of H_2O_2. This suggests that the pulse amplitude was directly correlated to peroxide formation without affecting the formation pathway, i.e. by increasing the discharge temperature.

3.3. Hydrogen peroxide production is independent from pulse steepness

Pulse steepness was also expected to affect the production of hydrogen peroxide. Fast rise times presumably result in an earlier initiation of discharges during pulse application and eventually larger discharge volumes while fast fall times are conducive for a more pronounced reillumination [24]. Accordingly, inception and reillumination statistics were investigated with respect to hydrogen peroxide production for rise times, t_{rise}, of 16 ns, 22 ns and 31 ns, and corresponding fall times, t_{fall}, of 21 ns, 29 ns and 37 ns. The pulse amplitude was set at 56 kV for an electrode distance, d, of 8 mm. Histograms for both statistics are presented in figure 6.

Each histogram includes measurements for 2700 discharge events. Probabilities, p, were expressed for the time of inception for different rise times with respect to the discharge beginning, t_{start}, or for the onset of reillumination, t_{min}, according to different fall times. Discharge inception for the shortest rise time, i.e. the steepest pulses, peaked (highest probability) at 25 ns, while the probability for a discharge inception later then 35 ns did not exceed 5%.

An increasing rise time resulted in a prolonged inception time from 30 ns and 32 ns, which was associated with a broadening of the probability distribution. Comparing the probability distributions for each rise time, it was reasonable to assume that the different maximum probabilities of 27% at 25 ns, 14% at 30 ns or 10% at 32 ns were a result of the different pulse shapes. In this respect, it should be mentioned again that the gradual decrease of voltage amplitudes during 100 ns pulses was more pronounced for shorter rise times, which was already described for figure 2(C). Correspondingly, probability distributions for inception shifted to later times and broadened.

Fall times mainly influenced the reillumination start. A narrow probability distribution for t_{min} with a width of 1 ns and a maximum of 45% at 4 ns was observed for the shortest rise and fall time. Similar to the inception probabilities, the maxima of the probability distributions were delayed from 5 ns and 7 ns and broadened for the longest rise and fall times.

Although pulse steepness did affect details of the discharge development, interestingly the overall propagation times, from discharge inception until onset of reillumination, were rather similar, i.e. between 69 ns and 71 ns, for all investigated conditions. The comparison of the comprehensive discharge

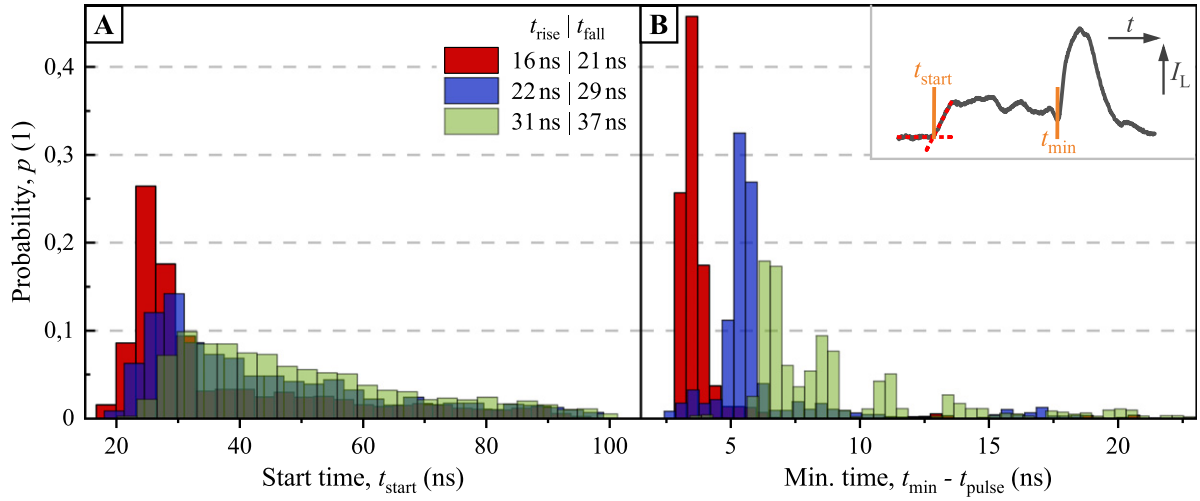

Figure 6. Probability distributions for inception times (panel (A)) and reillumination times (panel (B)) for an electrode distance, d, of 8 mm, a pulse amplitude, U_{mean}, of 56 kV and fall times, t_{fall}, of 21 ns (red bars), 29 ns (blue bars) as well as 37 ns (green bars). Altogether 2700 discharges were included in the analysis for each rise and fall time. Discharge inception was described by the time of first observable light emission, t_{start}, while the beginning of reillumination was associated with the time, t_{min}, when the discharge current changed polarity. For the shortest rise time, 27% of the discharges were incepted 25 ns into the applied high-voltage pulse and 45% of the discharges were reilluminating at 108 ns. Both probability distributions were broadened and delayed for increasing rise- and fall times.

development of 900 discharge events, i.e. summing up their individual propagation times, yielded also only marginally different total discharge propagation times between 62 µs and 64 µs. Accordingly, the corresponding times for radical production and discharge volumes were similar. This explains why no significant difference between the hydrogen peroxide production rates, k, of (147 ± 5) mmol l^{-1} s^{-1}, (143 ± 3) mmol l^{-1} s^{-1}, and (145 ± 7) mmol l^{-1} s^{-1} were observed for decreasing pulse steepness (figure S3). Mean discharge energies were likewise constant, consolidating previous results [24]. Summarily, an overall constant discharge propagation time resulted in a comparable hydrogen peroxide chemistry regardless of pulse steepness. Accordingly, a constant H_2O_2 production efficiency of (5.8 ± 0.1) g kWh^{-1} was typical for the application of 100 ns pulses with an amplitude of 56 kV.

Notably, this assessment only includes the application of high-voltage pulses, which resulted in a discharge event. Considering the probability of ignition by comparing the total number of applied pulses with the number of actual discharge events (2700 per pulse steepness) yielded a decreasing ignition probability of 58%, 33%, and 29% with increasing rise time (and associated increasing fall time). Taking the applied pulses with 'failed' ignition into account, hydrogen peroxide production rates would falsely be assumed to decrease to 85 mmol l^{-1} s^{-1}, 47 mmol l^{-1} s^{-1}, and 42 mmol l^{-1} s^{-1} when calculated with the number of pulses instead of discharge events. Overall, the ignition probability clearly needs to be considered and reported for the description of respective experiments to prevent wrongful conclusions on the production of reactive species for repetitively applied high-voltage pulses.

4. Discussion

Reaction chemistry for sub-microsecond pulsed streamer discharges in liquid water was investigated by quantifying the indicative hydrogen peroxide production depending on direct pulse parameters, i.e. pulse duration, pulse amplitude and pulse steepness. The highest peroxide production rate found was 9.2 g kWh^{-1}, which is higher than previously reported by comparable studies, e.g. ca. 2 g kWh^{-1} [9], 4.6 g kWh^{-1} [11], 0.8 g kWh^{-1} [1] or (0.46–3.64) g kWh^{-1} [6]. The difference to our results could conceivably be explained by the fact, that previous studies did not necessarily exclude applied high voltage pulses, which did not result in a discharge event and only contributed Ohmic losses. In addition, the comparison confirms the significance of a dedicated control of pulse parameters to improve the performance of the method. The best peroxide production rate found was 9.2 g kWh^{-1}, which is on the same order of magnitude but higher as in comparable studies [1, 6, 9, 11].

Dominant influence on H_2O_2 production could be attributed to pulse duration and pulse amplitude. An extended pulse duration eventually led to the stopping of discharge filaments, which was accompanied by decreased hydrogen peroxide production rates and efficiencies. A rather small increase in pulse amplitude of approximately 20% nearly doubled the energy dissipation and the production rate. Although pulse steepness did affect discharge developments, i.e. statistics of inception times and the contribution of the reillumination processes, and probably influenced the discharge inception, i.e. direct or indirect breakdown, as proposed in the literature, the respective effect on H_2O_2 production was marginal or negligible in com-

parison to pulse duration and amplitude [31, 32]. Altogether, production rates and achieved concentrations of species were primarily determined by differences in dissipated energies in relation to pulse parameters. However, the energy could not be arbitrarily increased for a given discharge structure but instead was eventually distributed in longer or more discharge channels. Accordingly, the overall discharge volume was crucial for an effective generation of species. This could explain the observed higher rates and efficiencies for hydrogen peroxide production for the application of higher pulse amplitudes and shorter pulse durations.

4.1. Discharge development depends on pulse parameters

For needle-to-plate geometries, plasma parameters, such as electron density and temperature have already been investigated. Although these studies rather investigated specific conditions but not a dedicated variation of pulse parameters, such as pulse durations, pulse amplitude or pulse steepness, selected settings were investigated for a range of several orders of magnitude, e.g. rise times of (0.1–100) ns, pulse amplitudes from (10–100) kV and pulse durations from 6 ns–10 µs. Nonetheless, electron densities were reported to be relatively stable between (10^{18}–10^{19}) cm^{-3} (with some outliers of (10^{17} and 10^{20}) cm^{-3}). Rotational temperatures of (2000–4000) K, black body radiation for temperatures of (7000–15 000) K, and electron energies of (1–3) eV were also reported [6, 30, 33–40]. These results present a good overview of pertinent plasma characteristics for sub-microsecond pulsed streamer discharges in liquid water and this study adds a detailed investigation on the dependency of electrical and optical plasma properties on pulse parameters.

Propagation time and streamer length of individual discharge channels were increasing with extended pulse duration (figure 2(B)). However, the start of a discharge was, on average, delayed by about 40 ns for longer pulses (figure 2(C)). Conversely, the onset of the reillumination occurred for rather similar delays for both pulse durations (figure 2(D)). Consequently, the propagation time was 2.8 times longer for the application of 300 ns pulses in comparison to 100 ns pulses.

According to literature, sub-microsecond pulsed streamer discharges in liquid water that were instigated with pulses with durations in the order of 100 ns propagate with a constant velocity of about 30 km s^{-1} [20, 22, 24]. This could be confirmed (figure 2(B)).

The typical propagation time of 62 ns for the application of 100 ns pulses corresponded to streamer lengths of 1.9 mm, while the filaments extend up to a typical length of 5.6 mm for a pulse duration of 300 ns (figure 2(B)). Individual channels could be much longer (but also shorter) since a typical inception time for the application of 300 ns pulses is prone to larger deviations from the mean (figure 2(C)).

Propagation times and resulting streamer length were to a lesser extend also depending on pulse amplitudes (figure 5(B)). Discharges were starting earlier during the application of a 100 ns pulse by 7 ns when pulse amplitudes were increased from 54 kV to 64 kV, which resulted in an increase in streamer length by 10%.

Pulse steepness, i.e. rise and fall times, had actually no significant effect on propagation times and streamer length. This finding was especially surprising, as previous studies showed a significant impact of the pulse rise time on discharge inception and an effect of pulse fall time on discharge reillumination [24, 31, 32]. A decreasing edge steepness impacted the discharge by a broadening of inception and reillumination time statistics. On average, discharge inception and the beginning of the reillumination phase were both delayed in a similar fashion (figure 6). Consequently, averaged propagation times turned out independent from rise or fall time.

Since the discharge channels are the origin for the generation of reactive species, the correlation of discharge expanse with H_2O_2 production is eminent. However, the actual discharge volume is also determined by the number of discharge channels and their distribution in addition to average (or maximal) streamer length. Unfortunately, these characteristics escape a statistical evaluation from 2D images. The respective assessment should be the dedicated topic of future studies, i.e. how streamer distribution and their individual properties depend on pulse parameters. However, some conclusions and conjectures were already possible without detailed information on the three dimensional discharge behavior. For pulses of about 100 ns duration, not only the extend of filaments that were originating along a thin wire at the center of a coaxial electrode system but also their number decreased when pulse amplitudes were lowered [10]. For the here investigated needle-to-plate geometry, this observation conceivably corresponded to the decrease in ignition probability for lower voltages. Concurrently, the number of filaments was possibly reduced and, accordingly, the overall discharge volume.

Images of the discharge development further show that discharge volumes and streamer lengths were not directly related for different pulse parameters (figure 2(A)). Discharge propagation and associated distribution of filaments were not generally isotropic or homogeneous. Instead, discharges exhibited a directionality toward the counter electrode for longer propagation times, which was, hence, more prominent for longer pulse durations of 300 ns. This resulted in an eventually decreasing growth rate of discharge volumes (figure 3).

For an isotropic propagation throughout the discharge development, a minimal electric field strength would have to be maintained in all directions to sustain ionization at all channel heads [24]. However, the electric field between a needle and plate is inherently inhomogeneous, decreasing away from the needle and more strongly for directions away from the needle axis [41]. Therefore, streamers heading directly toward the counter electrode were able to expand longer than streamers propagating in an askew direction, resulting in a decreased growth rate of the discharge volume. If the electric field fell below the critical field strength, continuous propagation stopped and instead a stepwise expansion ensued, provided that energy input into the channels is sustained [22].

4.2. Energy dissipation depends on discharge development

Discharges developed from the tip of the high-voltage electrode—originating from a distinct root point—as a single streamer, which could branch several times during its propagation with a constant velocity. The result was a complex morphology with distinct filaments, i.e. plasma channels connecting electrode and one of the streamer heads that either reached their full expansion (determined by propagation velocity and pulse duration) or already stopped earlier instead.

The production of reactive species and, therefore, the indicative amount of hydrogen peroxide was primarily depending on overall achieved discharge volumes. This volume was determined by the energy that could be provided into the discharge regardless of the underlying structure. The energy that was dissipated in a sub-microsecond pulsed streamer discharges in liquid water was found to depend linearly on the propagation time for a fixed set of operating parameters [24, 42]. Accordingly, the continuing extension of a filament by ionization, radiation, recombination processes, etc, needed a constant amount of energy for the same incremental growth. This assumption is supported by investigations on plasma parameters, e.g. electron density, temperatures and energies, which are relatively stable for different experimental settings [6, 30, 33–40]. The intrinsic discharge morphology can be described by an instructive 'single streamer' model, which summarizes the filamentous structure, including filament radii and number of heads, i.e. head-charges, by an unbranched 'single streamer' with a distinct discharge volume [24]. The constant rate of energy dissipation in a single streamer and the associated discharge volume, V_D, implies a limited number of filaments that can be included in this streamer because the expansion of each additional filament would have to dissipate additional energy that is not necessarily available. Conversely, an energy dissipation, which was increasing with pulse amplitude (figure 5(A)), combined with an insignificant change of streamer length, hence, had to be associated with an increasing number of filaments. Since energy dissipation rate and pulse amplitude were proportional, the correlation between the number of filaments and energy dissipation also had to be linear. Previous observations on the number of streamers in a coaxial discharge configuration that were increasing with applied pulse amplitudes support assumption and approach [10].

Consequently, hydrogen peroxide production should also depend in a similar fashion, i.e. linearly, on pulse durations, since propagation velocity and energy dissipation rate were constant (figure 4(B)). However, the H_2O_2-production rates and -efficiencies that were observed, were much lower than expected from the indeed lower energy that was dissipated for the longer pulses. The pronounced directionality of the streamers for 300 ns pulses toward the plate electrode offers an explanation in agreement with the 'single streamer' model.

The increasing inhomogeneity of the electric field across larger distances from the needle tip resulted in early stopping of filaments that went askew. This corresponded to a lower energy dissipation rate of about 25% for the 300 ns high-voltage pulses. This reduction is not sufficient to explain the actually much stronger decreasing hydrogen peroxide production rate by 50% or the production efficiency, which was smaller by 33% (figure 4). Instead, the results implicate a significantly reduced growth rate of discharge volume for discharges that were generated with 300 ns high-voltage pulses, in addition to the lower energy dissipation rate, in comparison with 100 ns high-voltage pulses. (Although overall discharge volumes were still larger for longer pulses.) On the one hand, filaments that stopped their propagation during the longer pulses could continue dissipating their share on the provided energy due to a step-wise propagation [22]. On the other hand, the filaments that continued propagation could branch whenever another filament stopped and, therefore, dissipated the still available energy, as this was required for a continued constant propagation according to the 'single streamer' model, but at the cost of a higher rate of energy dissipation for this 'forced' branching.

Filaments propagating sideways appeared rather dark, which seems contradictory to the hypothesized step-wise propagation. Filaments on a more direct trajectory to the counter electrode, which expanded for longer than 100 ns, showed instead additional branching as demanded by the 'single streamer' model. Accordingly, at a distance of 3–4 mm away from the needle tip, most of the filaments that came that far branched and branching became more likely for even larger distances. These filaments appeared brighter due to their extended propagation, i.e. light was emitted for longer times, and due to an increased current flowing through the existing channels to sustain ionization for the additional channel heads.

This was associated with a limited but higher conductivity of each remaining filament [7, 24]. Corresponding were a higher resistance and related greater resistive losses. The associated Joule heating scaled with filament length and quadratically with the current density within a discharge channel. Hence, if a filament of the streamer that propagated sideways stopped due to an insufficient electric field and simultaneously a filament directed toward the counter electrode branched, the energy for the continuing propagation of the latter became smaller. Accordingly, the energy available for expansion of the streamer decreased with every filament that stopped. Consequently, some filaments that were stopping did not induce further branching, i.e. fewer new filaments could be formed, corresponding to a reduced volume growth rate.

4.3. Hydrogen peroxide production depends on energy dissipation and discharge volume

The investigations revealed that the formation of reactive species and consequently hydrogen peroxide production depended on the discharge volumes, V_D, which could be established during the application of high-voltage pulses. A higher energy dissipation, which could be provided by either longer pulse durations or higher pulse amplitudes, was expended in an expanse of discharge volumes. This included, on the one hand, a larger extension away from the origin of streamers, i.e. the needle tip, and, on the other hand, encouraged branching of filaments.

The growth of individual discharge filaments was associated with a constant dissipation of energy per increase in

length. This resulted, for a fixed set of parameters, in a stable energy density within filaments and a corresponding steady radical production (per unit length). For increasing pulse amplitudes, the energy density still had to be stable but the energy dissipation rate grew. Accordingly, the number of filaments increased resulting in higher hydrogen peroxide production rates for 100 ns pulses (figure 5(B)).

A rigorous assessment of the filamentary discharge structures, depending on pulse duration and pulse amplitude, that were filling and determining the actual discharge volume, is currently difficult. However, maximum streamer lengths, L_s, and associated propagation times, Δt, provided a reasonable comparison (figure 3). Notably, the rate of increase in discharge volume slowed down for propagations times of more than 100 ns. This emphasizes the electric field at the streamer head as driving force of the streamer propagation. In the inhomogeneous needle-to-plate geometry, it became increasingly difficult to sustain ionization processes, especially away from the extended needle axis. In fact, filaments that were initially propagating at larger angles away from the needle tip eventually stopped (cf figure S2). Concurrently, the volume growth rate of the still propagating channels was reduced due to energy losses in the discharge. Notably, the increased channel temperature due to Joule heating, which is supposed to induce increased radical formation [6, 7, 9, 17], did not counteract the smaller volume growth rate and, consequently, hydrogen peroxide production rates decreased (figure 4).

As a consequence, the growth of discharge volume could be related to the amounts of hydrogen peroxide with typical production rates of (0.14 ± 0.02) mol l^{-1} s^{-1} for 100 ns pulses and (0.068 ± 0.004) mol l^{-1} s^{-1} for pulse durations of 300 ns (figure 4(A)). The two times lower rate for the longer pulse was explained by the reduced discharge volume growth rate due to an increasing directionality and associated fewer filaments. For an extended propagation period, the ratio between volume growth and energy dissipation rate of a discharge decreased. Therefore, not only the rate of hydrogen peroxide production was reduced but also the energy efficiency of the production. However, since the generation of sub-microsecond pulsed streamer discharges in liquid water depends on inhomogeneous electrode configurations, this instructs shorter pulse durations as more efficient (figure 4(B)).

5. Conclusions

The individual influence of three direct pulse parameter, i.e. pulse steepness, amplitude and duration, on the production of hydrogen peroxide in a sub-microsecond pulsed streamer discharges in liquid water could be investigated. The implementation of an optical and electrical diagnostic that could resolve the temporal development of individual discharges, e.g. automated determination of discharge currents and streamer length, facilitated an association between pulse parameter and hydrogen peroxide production. The energy dissipation rate in relation to the discharge volume were identified to primarily affect peroxide production rate and energy efficiency.

Increasing the energy dissipation rate, i.e. increasing the pulse amplitude, led to an increased hydrogen peroxide production rate with a constant production efficiency, as increasing numbers of filaments were formed. The stopping of channels due to an inhomogeneous electric field reduced the ratio between volume expansion and energy dissipation rate, which yielded lower hydrogen peroxide production rate and efficiency.

The relation between discharge volume and hydrogen peroxide was based on the statistical analysis of two-dimensional images, which revealed valuable structural characteristics of the discharge. However, a full 3D-reconstruction of the filamentary structure may enable an exact analysis of streamer quantity as well as quantification of occupied volume and may support the presented correlation. Our image analysis algorithm, which traces the discharge filaments, may provide the basis of such a reconstruction.

As the energy dissipation directly corresponds to increasing hydrogen peroxide production rates for increasing pulse amplitudes, the question arises for any application if there is a limit for this correlation and how much energy could be dissipated in a single discharge. Additionally, the method of increasing energy dissipation, e.g. via pulse amplitude, repetition frequency or water conductivity, may benefit the coupling between discharge energy and chemistry and should be investigated in more detail.

With respect to frequency, hydrogen peroxide was produced in the scope of this study by several hundred consecutive discharges. Hence the interaction between discharges and already existing hydrogen peroxide in solution could have reduced production rates. Therefore, an analysis of hydrogen peroxide production in single discharge events may be considered in the future.

Acknowledgments

The authors appreciate the research structure and the supportive background of the Leibniz Institute for Plasma Science and Technology (INP). Special thanks are given to Hans Höft for constructive discussions on experiments and data analysis.

Data availability statement

The data that support the findings of this study are available upon reasonable request from the authors.

ORCID iDs

Raphael Rataj https://orcid.org/0000-0002-7777-0367
Juergen F Kolb https://orcid.org/0000-0002-0434-5001

References

[1] Banaschik R, Lukes P, Miron C, Banaschik R, Pipa A V, Fricke K, Bednarski P J and Kolb J F 2017 *Electrochim. Acta* **245** 539–48

[2] Dang T H, Denat A, Lesaint O and Teissedre G 2008 *Plasma Sources Sci. Technol.* **17** 024013
[3] Schneider M, Rataj R, Kolb J F and Bláha L 2020 *Environ. Pollut.* **266** 115423
[4] Banaschik R, Jablonowski H, Bednarski P J and Kolb J F 2018 *J. Hazard. Mater.* **342** 651–60
[5] Kaufman F and Del Greco F P 1961 *J. Chem. Phys.* **35** 1895
[6] Locke B R and Shih K-Y 2011 *Plasma Sources Sci. Technol.* **20** 034006
[7] Locke B R and Thagard S M 2012 *Plasma Chem. Plasma Process.* **32** 875–917
[8] Banaschik R, Lukes P, Jablonowski H, Hammer M U, Weltmann K-D and Kolb J F 2015 *Water Res.* **84** 127
[9] Chauvet L, Nenbangkaeo C, Grosse K and Keudell A 2020 *Plasma Process. Polym.* **17** 1900192
[10] Banaschik R, Koch F, Kolb J F and Weltmann K-D 2014 *IEEE Trans. Plasma Sci.* **42** 2736–7
[11] Nguyen T S, Rond C, Vega A, Duten X and Forget S 2020 *Plasma Chem. Plasma Process.* **40** 955–69
[12] Joshi A A, Locke B R, Arce P and Finney W C 1995 *J. Hazard. Mater.* **41** 3–30
[13] Lukes P, Appleton A T and Locke B R 2004 *IEEE Trans. Ind. Appl.* **40** 60–7
[14] Yang S, Zhang L, Cui F and Ma J 2009 *2009 3rd Int. Conf. Bioinformatics and Biomedical Engineering* (Piscataway, NJ: IEEE) pp 1–4
[15] Li S, Hu S and Zhang H 2011 *IEEE Trans. Plasma Sci.* **40** 63–7
[16] Wen J, Li Y, Zhang M and Zhang G 2019 *2019 IEEE 20th Int. Conf. Dielectric Liquids (ICDL)* (Piscataway, NJ: IEEE) pp 1–4
[17] Medodovic S and Locke B R 2009 *J. Phys. D: Appl. Phys.* **42** 049801
[18] Palmer A W and House H 1972 *J. Phys. D: Appl. Phys.* **5** 1106
[19] Gzowski O A, Wlodarski R, Hesketh T R and Lewis T J 1966 *Br. J. Appl. Phys.* **17** 1483
[20] Marinov I, Guaitella O, Rousseau A and Starikovskaia S M 2013 *J. Phys. D: Appl. Phys.* **46** 464013
[21] Fujita H, Kanazawa S, Ohtani K, Komiya A, Kaneko T and Sato T 2014 *J. Appl. Phys.* **116** 213301
[22] Ceccato P H, Guaitella O, Le Gloahec M R and Rousseau A 2010 *J. Phys. D: Appl. Phys.* **43** 175202
[23] Seepersad Y, Fridman A and Dobrynin D 2015 *J. Phys. D: Appl. Phys.* **48** 424012
[24] Rataj R, Höft H and Kolb J F 2019 *Plasma Sources Sci. Technol.* **28** 125002
[25] Huiskamp T 2020 *Plasma Sources Sci. Technol.* **29** 023002
[26] Trojanowicz M 2009 *Anal. Chim. Acta* **653** 36–58
[27] Ricci F and Palleschi G 2005 *Biosens. Bioelectron.* **21** 389–407
[28] Šimek M, Hoffer P, Prukner V and Schmidt J 2020 *Plasma Sources Sci. Technol.* **29** 095001
[29] Pongrác B, Šimek M, Ondáč P, Člupek M, Babickỳ V and Lukeš P 2019 *Plasma Sources Sci. Technol.* **28** 02LT02
[30] Grosse K, Schulz-von der Gathen V and von Keudell A 2020 *Plasma Sources Sci. Technol.* **29** 095008
[31] Pekker M, Seepersad Y, Shneider M N, Fridman A and Dobrynin D 2013 *J. Phys. D: Appl. Phys.* **47** 025502
[32] Tereshonok D V, Babaeva N Y, Naidis G V and Smirnov B M 2016 *J. Phys. D: Appl. Phys.* **49** 505501
[33] An W, Baumung K and Bluhm H 2007 *J. Appl. Phys.* **101** 053302
[34] Salazar J N, Bonifaci N, Denat A and Lesaint O 2005 *2005 IEEE Int. Conf. Dielectric Liquids (ICDL)* (Piscataway, NJ: IEEE) p 91
[35] Namihira T, Sakai S, Yamaguchi T, Yamamoto K, Yamada C, Kiyan T, Sakugawa T, Katsuki S and Akiyama H 2007 *IEEE Trans. Plasma Sci.* **35** 614–8
[36] Šunka P 2001 *Phys. Plasmas* **8** 2587–94
[37] Dobrynin D, Seepersad Y, Pekker M, Shneider M, Friedman G and Fridman A 2013 *J. Phys. D: Appl. Phys.* **46** 105201
[38] Marinov I, Starikovskaia S and Rousseau A 2014 *J. Phys. D: Appl. Phys.* **47** 224017
[39] Pongrác B, Šimek M, Člupek M, Babickỳ V and Lukeš P 2018 *J. Phys. D: Appl. Phys.* **51** 124001
[40] Bruggeman P J *et al* 2016 *Plasma Sources Sci. Technol.* **25** 053002
[41] Deutsch W 1933 *Ann. Phys.* **408** 588–612
[42] Qin J and Pasko V P 2014 *J. Phys. D: Appl. Phys.* **47** 435202